ARTICLE

Detection of nanosecond time scale side-chain jumps in a protein dissolved in water/glycerol solvent

Jun Xu · Yi Xue · Nikolai R. Skrynnikov

Abstract In solution, the correlation time of the overall protein tumbling, τ_R, plays a role of a natural dynamics cutoff—internal motions with correlation times on the order of τ_R or longer cannot be reliably identified on the basis of spin relaxation data. It has been proposed some time ago that the 'observation window' of solution experiments can be expanded by changing the viscosity of solvent to raise the value of τ_R. To further explore this concept, we prepared a series of samples of α-spectrin SH3 domain in solvent with increasing concentration of glycerol. In addition to the conventional ^{15}N labeling, the protein was labeled in the Val, Leu methyl positions ($^{13}CHD_2$ on a deuterated background). The collected relaxation data were used in asymmetric fashion: backbone ^{15}N relaxation rates were used to determine τ_R across the series of samples, while methyl ^{13}C data were used to probe local dynamics (side-chain motions). In interpreting the results, it has been initially suggested that addition of glycerol leads only to increases in τ_R, whereas local motional parameters remain unchanged. Thus the data from multiple samples can be analyzed jointly, with τ_R playing the role of experimentally controlled variable. Based on this concept, the extended model-free model was constructed with the intent to capture the effect of ns time-scale rotameric jumps in valine and leucine side chains. Using this model, we made a positive identification of nanosecond dynamics in Val-23 where ns motions were already observed earlier. In several other cases, however, only tentative identification was possible. The lack of definitive results was due to the approximate character of the model—contrary to what has been assumed, addition of glycerol led to a gradual 'stiffening' of the protein. This and other observations also shed light on the interaction of the protein with glycerol, which is one of the naturally occurring osmoprotectants. In particular, it has been found that the overall protein tumbling is controlled by the bulk solvent, and not by a thin solvation layer which contains a higher proportion of water.

Keywords α-Spectrin SH3 domain · α-ketoisovalerate labeling · Backbone ^{15}N and methyl ^{13}C relaxation · Extended Lipari–Szabo model · Solvent slaving · Preferential hydration

Introduction

Inside a living organism, proteins exist and function in a variety of different environments. Some float freely in a solution, which can be more crowded and viscous (cytosol) or less so (extracellular fluid). Others are embedded in membranes. Yet others operate as a part of protein assemblies such as ribosome or proteasome and are, therefore, wedged between partner proteins. Protein assemblies are often immobilized to a greater or lesser degree. However, even in the most constricted environment, such as mineralized collagene, proteins display a significant amount of non-trivial internal dynamics.

Protein environment (matrix) has a strong—often definitive—influence on protein structure, dynamics, and function. In addition, in the context of NMR studies, it determines the boundary between the solution- and solid-state situations. It is this latter spectroscopic aspect that motivates this study. In solution, the correlation time of the overall protein tumbling, τ_R, plays a role of a natural

J. Xu · Y. Xue · N. R. Skrynnikov (✉)
Department of Chemistry, Purdue University,
560 Oval Drive, West Lafayette, IN 47907-2084, USA
e-mail: nikolai@purdue.edu

dynamics cutoff. The internal motions that occur on a time scale faster than τ_R can be successfully captured by solution relaxation experiments, whereas the slower motions are effectively 'masked' and remain unobservable. In solids, there are no such limitations—anisotropic interactions (dipolar, CSA, and quadrupolar) can, in principle, provide information on motional processes over a wide range of time scales.

It has been recognized some time ago by Lienin et al. (1998) that the 'observation window' of solution experiments can be expanded by changing the viscosity of the solvent to push upward the value of τ_R. Later, Zeeb et al. (2003) pursued this agenda in their study of the cold shock protein CspB. The ^{15}N relaxation data acquired from three samples of CspB in water/ethylene glycol mixtures were analyzed using a model-free approach (Lipari and Szabo 1982a). As it turned out, the majority of the secondary-structure residues could be adequately fitted using a simple Lipari–Szabo model. The extracted order parameters S_f^2 showed little variation with the concentration of ethylene glycol, thus lending support to the idea that τ_R can be re-defined without perturbing the internal dynamics. At the same time, fourteen residues showed big changes in fast-motion correlation times: from ~ 50 ps to ~ 1 ns. Furthermore, at a high concentration of ethylene glycol five residues showed a preference for the extended Lipari–Szabo model (Clore et al. 1990b). The significance of these findings is not completely clear—they may indicate the increased sensitivity of the relaxation data to nanosecond time-scale internal motions or, alternatively, point toward the slow-down of internal dynamics caused by ethylene glycol.[1] The uncertainty surrounding this result is not surprising—nanosecond time-scale motions in a protein backbone are notoriously difficult to detect, even with good quality data available at multiple magnetic fields (Chen et al. 2004). A moderate increase in τ_R achieved by adding ethylene glycol—to 17.3 ns—does not resolve this conundrum (Chevelkov et al. 2007).

Building upon the work of Zeeb et al., Korchuganov et al. (2004) undertook a combined interpretation of the ^{15}N relaxation data obtained from four water/glycerol samples of barnase. In agreement with the previous findings, the authors noted that only a small fraction of residues is possibly affected by the presence of glycerol. The majority shows simple Lipari–Szabo dynamics, with S_f^2 and τ_f essentially independent of the glycerol concentration. The results of the joint analysis employing the data from the four

samples were used to determine the τ_R value in the limit of zero glycerol concentration.[2] Thus, the expanded 'dynamic window' of the viscous samples has been used only indirectly as the researchers focused on the global tumbling time, τ_R.

In this work we expand the scope of the previous studies by measuring both backbone ^{15}N and side-chain methyl ^{13}C relaxation in a series of samples with progressively increased viscosity. This approach offers several new perspectives. First, methyl relaxation properties are superior to the backbone, ensuring high quality of the data and accurate characterization of local dynamics. Second, τ_R determination (based on the backbone ^{15}N data) can now be separated from the analysis of internal motions (side-chain ^{13}C data). Third, side-chain data offer better opportunities for detection of nanosecond time-scale dynamics. Indeed, side-chain rotameric jumps are a distinctive motional process which provides a clear signature in terms of spin relaxation (Nicholson et al. 1992; Skrynnikov et al. 2002; Reif et al. 2006). Fourth, if the matrix is to exert any influence on protein internal motions, methyl-bearing side chains offer an excellent chance to quantify this effect. While backbone amide sites mostly fall in the narrow range $S_f^2 \sim 0.7 - 0.9$, side-chain methyls show much wider variation, $S_f^2 \sim 0.2 - 0.9$. Furthermore, fast-motion correlation times τ_f that cannot be reliably determined in amides are well defined in methyls, spanning the range from ~ 20 to ~ 120 ps (Xue et al. 2007). All this makes methyls a superior probe of protein dynamics, including dynamic responses to various perturbations such as point mutations (Millet et al. 2003; Mittermaier and Kay 2004; Clarkson and Lee 2004; Igumenova et al. 2005), ligand binding (Kay et al. 1996; Finerty et al. 2002; Johnson et al. 2006; Frederick et al. 2007), pH variations (Hu et al. 2003), etc. In the context of the present study it is particularly interesting to find out whether water/glycerol solvent causes any significant change in side-chain dynamics. Recently we were able to show that native methyl dynamics is essentially preserved in transition from solution to a well-hydrated protein crystal (Agarwal et al. 2008). Given the role of glycerol as a popular cryoprotectant in protein crystallography and in solid-state NMR (Rariy and Klibanov 1997; Kempkes et al. 2008), it is interesting to see whether the same claim can be made about the water/glycerol environment.

---

[1] An additional complication arises from the fact that CspB is thoroughly affected by ms time scale exchange arising from the folding–unfolding equilibrium that exists in this marginally stable protein. Addition of ethylene glycol shifts this equilibrium toward the folded form and thus alters the R_{ex} rates.

[2] In order to extrapolate the results toward the limit of zero glycerol concentration the authors relied on the data from translational diffusion measurements. It should be pointed out that these measurements can be technically demanding; their accuracy is typically much lower than that of the standard τ_R determination (Price 1998). In addition, a simple relationship between the translational and rotational diffusion coefficients, in principle, can be violated as a result of the solvent partition (i.e. preferential hydration of the protein surface).

Materials and methods

Protein sample

The study was conducted on a small globular protein, chicken α-spectrin SH3 domain (α-spc SH3), which has been well characterized by X-ray crystallography, as well as solution- and solid-state NMR (Musacchio et al. 1992; Blanco et al. 1997; Castellani et al. 2002). Selective labeling of Leu, Val methyl groups was achieved by adding an α-ketoisovalerate to the expression media. α-ketoisovalerate with the labeling scheme $^{13}CHD_2-CH(^{13}CHD_2)-CO-COO^-$ was purchased from Isotec and deuterated at the position 3 as described previously (Goto et al. 1999). The protein was expressed in D_2O-based media containing 100 mg/L of labeled α-ketoisovalerate, 2 g/L deuterated D-glucose, and 1 g/L $^{15}NH_4Cl$.

The sample was originally prepared by dissolving α-spc SH3 to the concentration 1.8 mM in 90% H_2O–10% D_2O (unbuffered, pH 3.5). Incremental amounts of d_5-glycerol (Isotec) were added to the initial sample to produce the following solvent compositions: 0, 26, 39% (duplicate), 54, and 59% w/w glycerol concentration. In doing so, the desired amount of (pre-heated) glycerol was weighed in an Eppendorf tube, the protein sample was subsequently transferred into the same tube, and the solution was mixed by vortexing. Note that the exact amount of glycerol (subject to a substantial uncertainty) is of no critical importance in our study since τ_R is determined directly from the analysis of the ^{15}N relaxation data; the information on macroscopic viscosity of the given water/glycerol composition is used only in general discussion.

Relaxation measurements

All experiments were conducted at 30°C, static magnetic field strength 14.1 T (600 MHz). Backbone ^{15}N relaxation data were collected using the standard suite of experiments (Farrow et al. 1994; Korzhnev et al. 2002; Hansen and Kay 2007). The absence of the R_{ex} contribution into transverse relaxation in all residues except Asp 48 was confirmed by ^{15}N relaxation dispersion measurement (Tollinger et al. 2001). Side-chain methyl ^{13}C R_1 and $R_{1\rho}$ data were recorded using the pulse sequences fashioned from the standard ^{15}N experiments, as appropriate for the 2-spin $^{13}CHD_2$ system. The details of the pulse sequences have been recently reported (Agarwal et al. 2008). The quality of the ^{13}C relaxation data remains excellent even at high glycerol concentration, as illustrated in Fig. 1. The exceptional quality of the spectra obtained with this particular isotopic labeling scheme has been previously noted for high-molecular-weight proteins and protein assemblies (Tugarinov and Kay 2005; Tugarinov et al. 2006).

Data interpretation: spectral densities

The data analysis relied on the standard Lipari–Szabo expressions for the correlation function $g(t)$ and the spectral density $J(\omega)$ (Lipari and Szabo 1982a):

$$g(t) = \left\{ \alpha S_f^2 + \left(1 - \alpha S_f^2 \right) e^{-t/\tau_f} \right\} e^{-t/\tau_R^{\mathrm{eff}}} \quad (1.1)$$

$$J(\omega) = \alpha S_f^2 \frac{\tau_R^{\mathrm{eff}}}{1 + (\omega \tau_R^{\mathrm{eff}})^2} + \left(1 - \alpha S_f^2 \right) \frac{\tau}{1 + (\omega \tau)^2} \quad (1.2)$$

$$1/\tau = \left(1/\tau_f \right) + \left(1/\tau_R^{\mathrm{eff}} \right) \quad (1.3)$$

This model is parametrized with two variables—fast motion order-parameter S_f^2 and local correlation time τ_f—and is accordingly termed the LS-2 model (Skrynnikov et al. 2002). The parameter α is included to facilitate the comparison between the backbone and methyl results. In the case of the methyl $^{13}C-^1H$ ($^{13}C-^2H$) dipolar interactions, α is set to 1/9 to factor out the effect of fast methyl rotation (Lipari and Szabo 1982b; Ishima et al. 2001); for all other interactions α is equal to 1. The correlation time τ_R^{eff} was

Fig. 1 Typical methyl ^{13}C relaxation curves from 59% glycerol sample. To select the representative example, the relaxation data were sorted according to the fitting residual and one methyl group, Val 9 γ1, was picked from the middle of the list
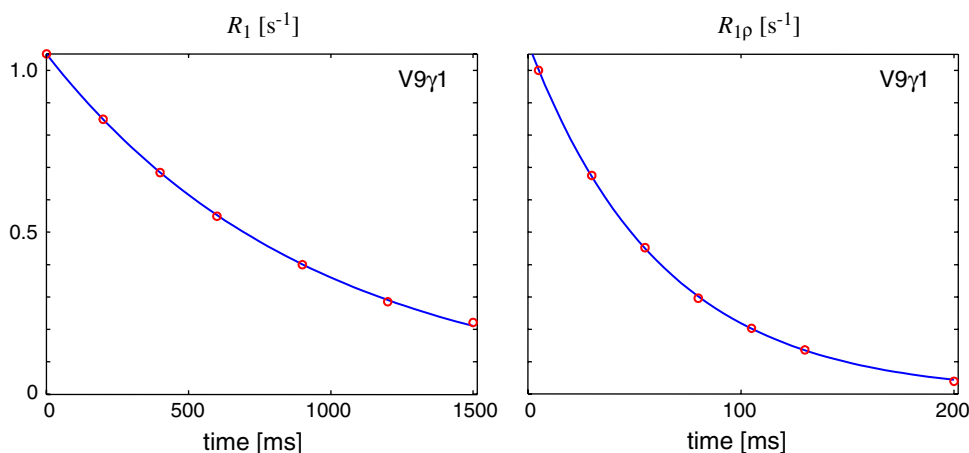
modified to account for the effect of (presumed axially symmetric) tumbling anisotropy (Lee et al. 1997):

$$\tau_R^{\text{eff}} = \xi\tau_R = \xi(6D_{\text{iso}})^{-1} \tag{2.1}$$

$$\xi = \left(1 - \frac{(D_{\parallel}/D_{\perp}) - 1}{(D_{\parallel}/D_{\perp}) + 2} \cdot \frac{3\cos^2\theta - 1}{2}\right)^{-1} \tag{2.2}$$

where θ is the angle between the interaction axis and the unique axis of the rotational diffusion tensor. The values of θ have been determined individually for different interactions; in doing so it was assumed that (1) the ^{15}N–^{1}H^N dipolar vector is oriented along the corresponding bond, (2) the long axis of the ^{15}N CSA tensor lies in the peptide plane and makes a 20° angle with the N–H^N bond (Cornilescu and Bax 2000), (3) the methyl ^{13}C–^{1}H^N dipolar vector is effectively oriented along the methyl threefold symmetry axis, after fast methyl rotation is factored in, and the same is true for the methyl ^{13}C CSA long axis. The calculations were carried out using a high-resolution crystallographic structure 1U06 (Chevelkov et al. 2005); for several side-chains showing alternate conformations the coefficients ξ were averaged accordingly. While there is no precise way to calculate ξ in the case of a side chain that populates multiple conformations, the above approach provides a reasonable approximation. In any event, the role of tumbling anisotropy in α-spc SH3 is limited—for instance, the methyl groups investigated in this work have ξ values ranging from 0.97 to 1.07. As an alternative to τ_R^{eff}, the effect of anisotropy can also be included via the following construct, $g(t) = \left\{\alpha S_f^2 + \left(1 - \alpha S_f^2\right)e^{-t/\tau_f}\right\}g_{\text{Woessner}}(t)$, which makes use of the Woessner's result for anisotropic rotator (Woessner 1962; Lipari and Szabo 1982a). Our calculations show that in the case of α-spc SH3 the two methods produce essentially identical results.

To address spin relaxation induced by slower (nanosecond) time scale rotameric jumps in Val and Leu side chains, we resorted to the extended Lipari–Szabo model (Clore et al. 1990a, b) which has been somewhat reformulated compared to the original version (Skrynnikov et al. 2002):

$$\begin{aligned} g(t) = &\left\{\alpha S_f^2 + \left(1 - \alpha S_f^2\right)e^{-t/\tau_f}\right\} \\ &\times \left\{S_s^2 + (1 - S_s^2)e^{-t/\tau_s}\right\}e^{-t/\tau_R^{\text{eff}}} \end{aligned} \tag{3.1}$$

$$\begin{aligned} J(\omega) = &\alpha S_f^2 S_s^2 \frac{\tau_R^{\text{eff}}}{1 + (\omega\tau_R^{\text{eff}})^2} + \alpha S_f^2(1 - S_s^2)\frac{\tau_1}{1 + (\omega\tau_1)^2} \\ &+ \left(1 - \alpha S_f^2\right)S_s^2 \frac{\tau_2}{1 + (\omega\tau_2)^2} \\ &+ \left(1 - \alpha S_f^2\right)(1 - S_s^2)\frac{\tau_3}{1 + (\omega\tau_3)^2} \end{aligned} \tag{3.2}$$

$$1/\tau_1 = (1/\tau_s) + \left(1/\tau_R^{\text{eff}}\right) \tag{3.3}$$

$$1/\tau_2 = \left(1/\tau_f\right) + \left(1/\tau_R^{\text{eff}}\right) \tag{3.4}$$

$$1/\tau_3 = \left(1/\tau_f\right) + (1/\tau_s) + \left(1/\tau_R^{\text{eff}}\right) \tag{3.5}$$

The model (3) involves four parameters pertaining to local dynamics—S_f^2, τ_f, S_s^2, and τ_s—and is referred to as the LS-4 model (Skrynnikov et al. 2002).

Data interpretation: rotational diffusion tensor

The starting point in the determination of the diffusion tensor was a set of ^{15}N R_1, R_2, and NOE data measured by us at 500 and 600 MHz in water solution at 7°C (Chevelkov et al. 2007). The set was edited to remove eleven residues with NOE < 0.7 and one residue which showed significant exchange broadening. Consequently, a comprehensive optimization procedure was launched to refine both local motional parameters, S_f^2 and τ_f, and the overall rotational diffusion tensor. The procedure has been designed similar to the well-established approach (Li and Montelione 1995; Mandel et al. 1995; Cole and Loria 2003), where the local and the global motional parameters are optimized in an iterative fashion. The distinctive feature of our protocol is that the diffusion tensor at each step is optimized using the R_2/R_1 ratios. In contrast to the earlier work (Tjandra et al. 1995, 1996), these ratios are calculated using the complete form of the spectral density function, (1.2), including residue-specific S_f^2 and τ_f values. The advantage of this design is the rapid convergence of the iterative optimization scheme. The following parameters pertaining to the rotational diffusion tensor have been extracted: $D_{\parallel}/D_{\perp} = 1.20$, $\Theta = 40°$, $\Phi = 107°$, where the latter two parameters denote the directional angles of the diffusion tensor long axis in the coordinate frame of the structure 1U06.

Next, we characterized the rotational diffusion in a series of samples with increasing concentration of glycerol. Given that (1) only R_1 and R_2 data at the single magnetic field strength were available for each of these samples, and (2) the quality of the backbone data deteriorates visibly with increasing solvent viscosity, most of the parameters were fixed according to the previous findings. Specifically, $D_{\parallel}/D_{\perp}$, Θ, Φ, selection of residues used for determination of the diffusion tensor, and their respective S_f^2, τ_f values were all used as obtained previously. The optimization was limited to a single variable, D_{iso}, which was adjusted according to the R_2/R_1 ratios. Use of the residue-specific S_f^2, τ_f parameters in the R_2/R_1 analyses resulted in up to a 3% increase in the determined τ_R values. While it is fully expected that S_f^2 and τ_f, as well as other parameters such as $D_{\parallel}/D_{\perp}$, are changed slightly upon addition of glycerol,
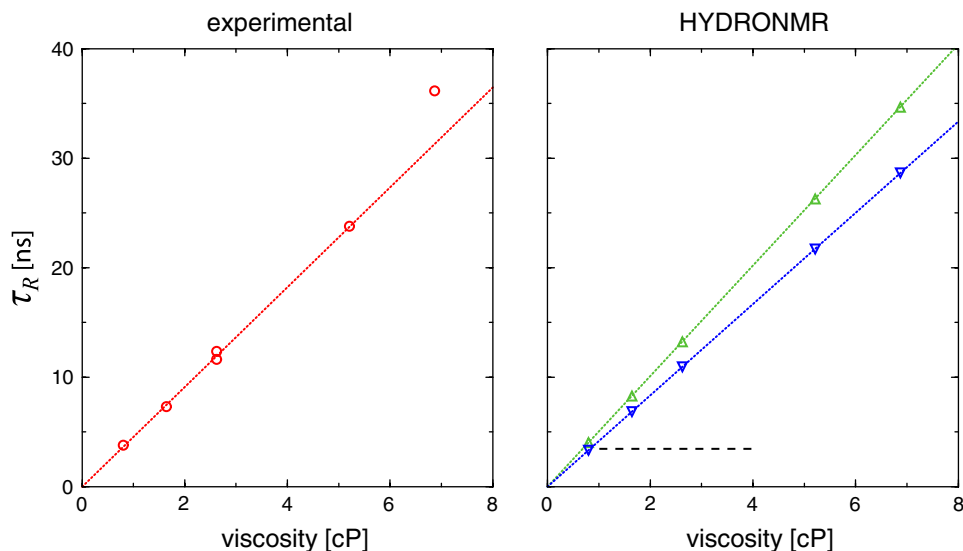
Fig. 2 Overall tumbling correlation time of α-spc SH3 in water/glycerol solvent as determined from the experimental ^{15}N relaxation data (*left part*) and HYDRONMR (de la Torre et al. 2000b) calculations (*right part*). Viscosity values are obtained from the reference tables (Chemical Rubber Company 1948) based on the glycerol concentration in the six experimentally studied samples; the same values are then used as an input for the HYDRONMR calculations. In the subsequent analysis of methyl relaxation data we avoid using the error-prone viscosity values and rely instead on the accurately determined τ_R. The protein coordinates used in the HYDRONMR calculations are from the recently reported MD trajectory of α-spc SH3 (Chevelkov et al. 2007) (*upright triangles*) and from the NMR structure 1AEY (Blanco et al. 1997) (*inverted triangles*). The horizontal dashed line in the right half of the plot serves the purpose of discussion

these changes should not have any material impact on the determination of D_{iso} and the subsequent treatment of methyl relaxation.

The extracted $\tau_R = 1/6D_{iso}$ values are plotted in Fig. 2 (left part) as a function of the estimated solvent viscosity. Since these data are relevant for the discussion of preferential hydration (see below), we have also calculated τ_R values using the HYDRONMR program (de la Torre et al. 2000b). The calculations are somewhat less than straightforward because α-spc SH3 domain contains a flexible N-terminus which is missing from both crystallographic and NMR structures of the protein. The calculation using the NMR structure 1AEY (Blanco et al. 1997), which misses four N-terminal residues, results in the slightly underestimated τ_R values (downward pointing triangles in the right part of Fig. 2). On the other hand, the calculation using a full-length protein—a randomly selected snapshot from the recently reported MD trajectory of α-spc SH3 (Chevelkov et al. 2007)—leads to the somewhat overestimated values (upright triangles). The latter result can be expected since the extended N-terminus is treated by the HYDRONMR program as rigid.

Statistical tests

To assess the performance of the LS-2 and -4 models we used the second-order variant of the Akaike Information Criterion (AIC) (Akaike 1973; Hurvich and Tsai 1989), as appropriate for small samples (number of fitted points $N < 40$; Burnham and Anderson 2002):

$$AIC_c = N \ln \chi^2 + 2K + \frac{2K(K+1)}{N-K-1} \tag{4.1}$$

$$\chi^2 = \frac{1}{N} \sum_{i=1}^{N} \left(\frac{\Gamma_i^{fit} - \Gamma_i^{exptl}}{\Gamma_i^{exptl}} \right)^2 \tag{4.2}$$

where Γ_i denote the relaxation rates and K is the number of fitted model parameters plus one. More details on application of AIC are given below.

Results and discussion

Methyl ^{13}C relaxation: LS-2 interpretation

Methyl ^{13}C relaxation in the α-ketoisovalerate-derived sample with deuterated background and selective incorporation of ^{13}C, ^{1}H spins is driven by ^{1}H–^{13}C and ^{2}H–^{13}C dipolar interactions across a single bond as well as ^{13}C CSA interaction. The relevant expressions for R_1 and R_2 relaxation rates have been cited in the literature along with the recommended values of the interaction constants (Ishima et al. 2001; Agarwal et al. 2008). The relative contributions of the three relaxation mechanisms into methyl ^{13}C R_1 rates are, on average, 86, 13, and 1%, respectively (determined from the experimental data collected in this study,

Table 1 Classification of models used for analysis of side-chain dynamics

Model[a]	Fitting parameters[b]	K[c]	N[d]
LS-2(m)	S_f^2, τ_f	3	12
LS-2(sc)	$S_f^2(1)$, $\tau_f(1)$, $S_f^2(2)$, $\tau_f(2)$	5	24
LS-4(m)	S_f^2, τ_f S_s^2, τ_s	5	12
LS-4(sc)	$S_f^2(1)$, $\tau_f(1)$, $S_f^2(2)$, $\tau_f(2)$ $S_s^2(1)$, $\tau_s(1)$, $S_s^2(2)$, $\tau_s(2)$	9	24
LS-4(sc-red)	$S_f^2(1)$, $\tau_f(1)$, $S_f^2(2)$, $\tau_f(2)$ S_s^2, τ_s	7	24

[a] All models listed in this table assume that the protein internal dynamics does not change upon addition of glycerol. Alternatively, we also use a standard Lipari–Szabo model to interpret ^{13}C R_1 and R_2 rates (two values measured at a given glycerol concentration) in terms of S_f^2 and τ_f

[b] Indices (1) and (2) refer to two methyl sites in Val and Leu side chains

[c] Number of fitting parameters plus one, as used in the AIC evaluation

[d] Number of experimental points available in this study is 12 points per methyl. The exceptions are Leu-33 $\delta 1$, Leu-34 $\delta 1$ (10 points per methyl) and Leu-8 $\delta 2$, Leu-61 $\delta 2$ (4 points per methyl). The missing data are due to the spectral overlaps that occur at certain glycerol concentrations

600 MHz). For methyl ^{13}C R_2 rates the corresponding proportions are 81, 11, and 8%.

The central idea of this study is to engineer a situation where τ_R plays a role of the experimentally controlled variable, whereas all other dynamic parameters remain constant. In accordance with this agenda, we analyze the series of ^{13}C R_1 and R_2 relaxation rates from a given methyl group in six samples with progressively increasing τ_R. The values of τ_R and $\tau_R^{\text{eff}} = \xi \tau_R$ are obtained from the analysis of the backbone ^{15}N relaxation data (see "Materials and methods") and are assumed to be known. The local motional parameters are assumed to be insensitive to the glycerol content of the sample and are treated as fitting parameters. If the standard Lipari–Szabo model is applied, (1), this translates into two fitting parameters and 12 experimentally measured points per methyl group. In what follows such interpretation is termed LS-2(m) where the descriptor (m) indicates that the model is applied to all data from a selected methyl. The summary of the LS-2(m) parameters can be found in Table 1.

Application of the LS-2(m) model to carbon relaxation data collected in this study led to the separation of all methyl groups into three classes, designated A, B, and C. The class A methyls were successfully fitted using the LS-2(m) model, as illustrated in Fig. 3. The red circles in the plot represent the experimental data, while the blue squares represent the results of the least-square fitting procedure (the connecting lines are added to enhance the visualization of the data). The extracted motional parameters are $S_f^2 = 0.80$, $\tau_f = 55$ ps and $S_f^2 = 0.79$, $\tau_f = 20$ ps for Val-9 $\gamma 1$ and $\gamma 2$, respectively. This correlates reasonably well with the results of ^2H

Fig. 3 Fitting of the methyl ^{13}C relaxation data from Val-9 $\gamma 1$ and $\gamma 2$ with LS-2(m) model (*red circles*—experimental rates, *blue squares*—best-fit rates)
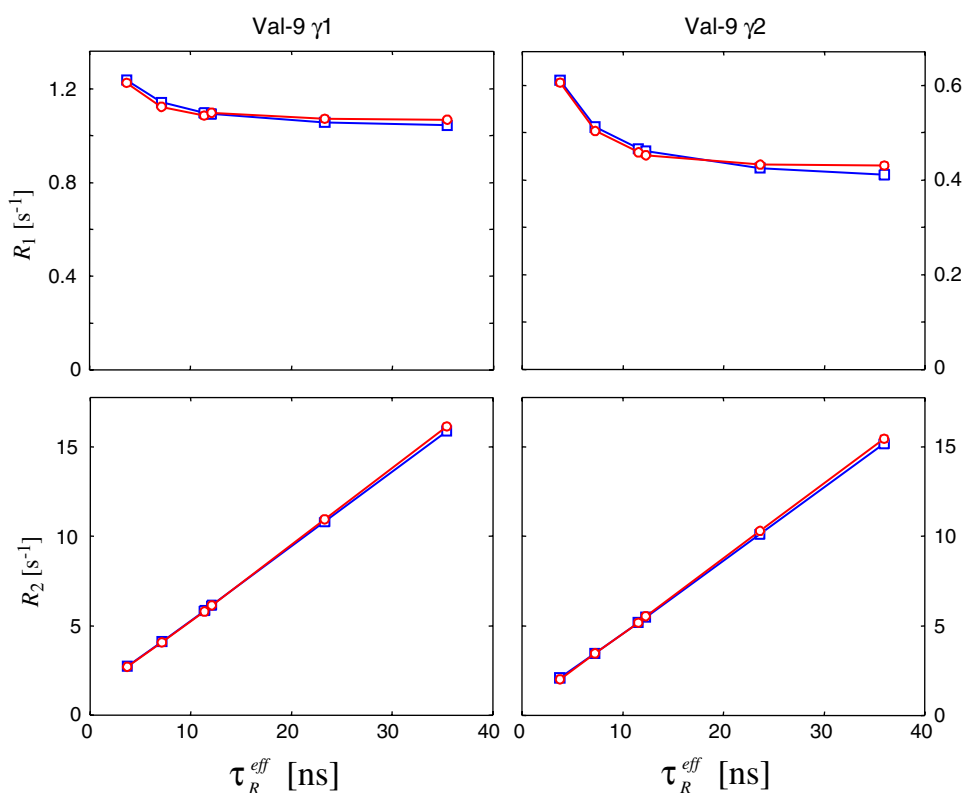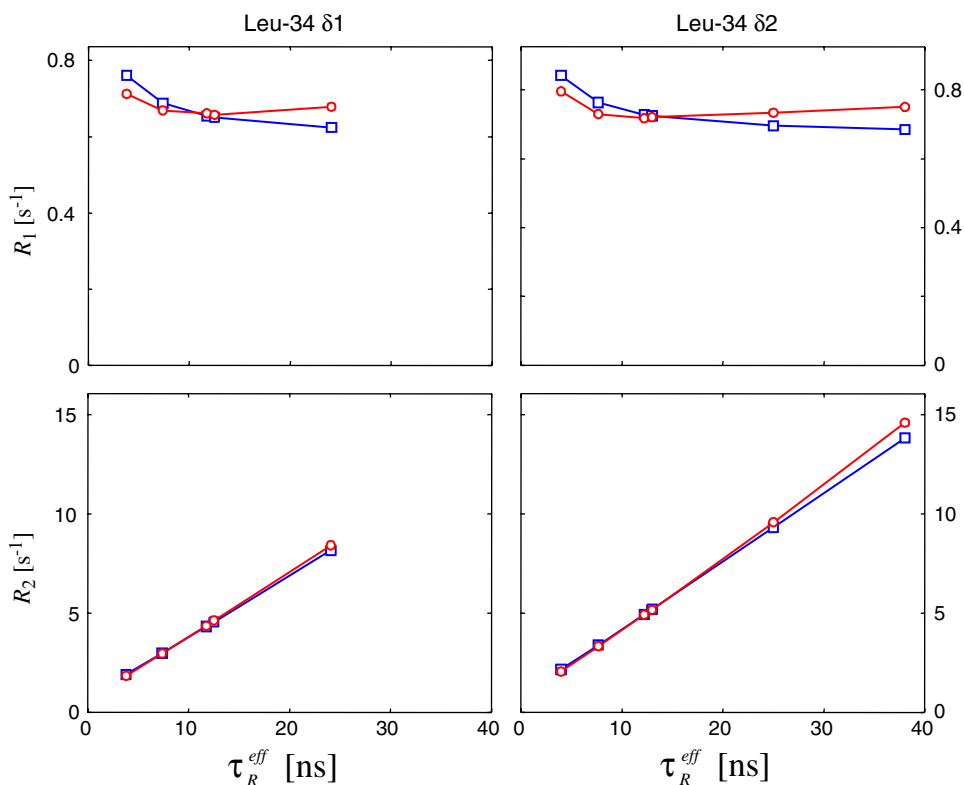
Fig. 4 Fitting of the methyl ^{13}C relaxation data from Leu-34 $\delta1$ and $\delta2$ with LS-2(m) model. The data for $\delta1$ are incomplete due to the spectral overlap at high glycerol concentration

relaxation study conducted at lower temperature (10°C): $S_f^2 = 0.82$, $\tau_f = 90$ ps and $S_f^2 = 0.75$, $\tau_f = 30$ ps (Reif et al. 2006). As it turns out, the examples of such successful fitting are rare—in fact, Val-9 represents the only convincing case (and even there slight systematic deviations can be easily discerned in the plot).

A more populous group, class B, shows a distinct divergence pattern between the experimental and fitted rates, Fig. 4. Clearly, some systematic factors are at play in shaping the R_1, R_2 profiles for these sites. The explanation that most readily comes to mind is that the local dynamic parameters actually change with increase in glycerol concentration (i.e. the key assumption of the LS-2(m) model is not entirely valid). To test this hypothesis, we fitted R_1 and R_2 values at each glycerol concentration with the LS-2 model, thus extracting *glycerol-concentration-dependent* S_f^2 and τ_f. The fitting in this case involves only two data points and two adjustable parameters, so that the residual χ^2 turns into zero. However, even a minimum set of methyl relaxation data can be reliably interpreted using a simple Lipari–Szabo model (Ishima et al. 2001; Millet et al. 2002) and our data are sufficiently precise to support such interpretation.

The outcome of this point-by-point analysis is presented in Fig. 5. Indeed, as expected, S_f^2 and τ_f show modest increases with increase in glycerol concentration. In particular, for Leu-34 $\delta2$ S_f^2 increases from 0.64 to 0.70, while τ_f rises more substantially, from 32 to 38 ps. Considering the

results shown in Fig. 5, one could argue that both τ_R (x-axes) and S_f^2, τ_f (y-axes) respond to the changes in the water/glycerol environment. The increasing amount of glycerol slows down the overall tumbling and, at the same time, leads to the 'stiffening' of the protein. Hence a linear character of the relationship between τ_R on one hand and S_f^2, τ_f on the other hand, as demonstrated in Fig. 5. The same behavior is observed in other methyls belonging to this class: Leu-8, Leu-10, Leu-12, Leu-31 $\delta2$, Leu-33, Val-44, and Leu-61. Of note, the linearity of S_f^2, τ_f vs. τ_R generally holds for these residues, with no evidence of any 'phase transition'.

It has been demonstrated before that the glycerol solvent, with its tight hydrogen bonding network, has a stifling effect on protein internal dynamics [cf. the concept of solvent 'slaving' (Fenimore et al. 2002)]. The data along these lines have been obtained from Raman and neutron scattering experiments (Caliskan et al. 2004), disulfide trapping studies (Butler and Falke 1996), and NMR amide exchange measurements (Foord and Leatherbarrow 1998; Knubovets et al. 1999). In their MD simulation study, Tarek and Tobias (2008) noted that substituting glycerol for water scales down the amplitudes of internal motions, yet preserves the native character of protein dynamics (distinct from that found in a dried protein). Priev et al. (1996) used their adiabatic compressibility data to estimate that addition of 35% (w/w) glycerol reduces the *rms* amplitude of protein atom fluctuations by 0.06 Å. Our S_f^2, τ_f data (Fig. 5) add to this body of evidence and point at the

Fig. 5 S_f^2 and τ_f parameters as extracted from point-by-point analysis of the Leu-34 relaxation data shown in Fig. 4
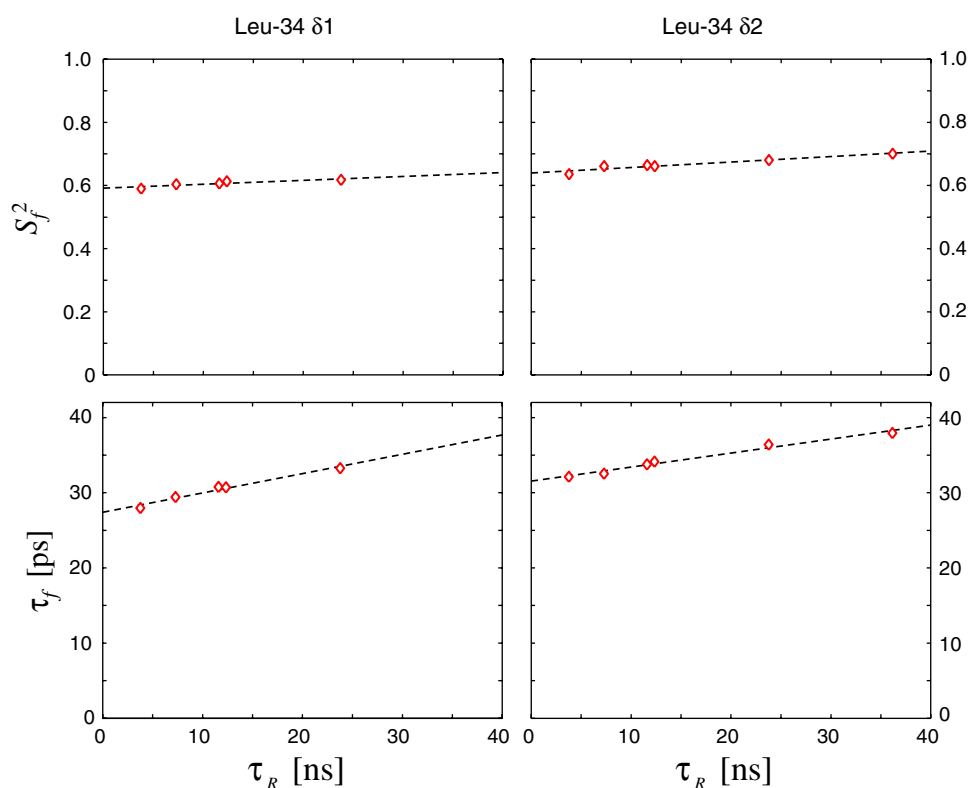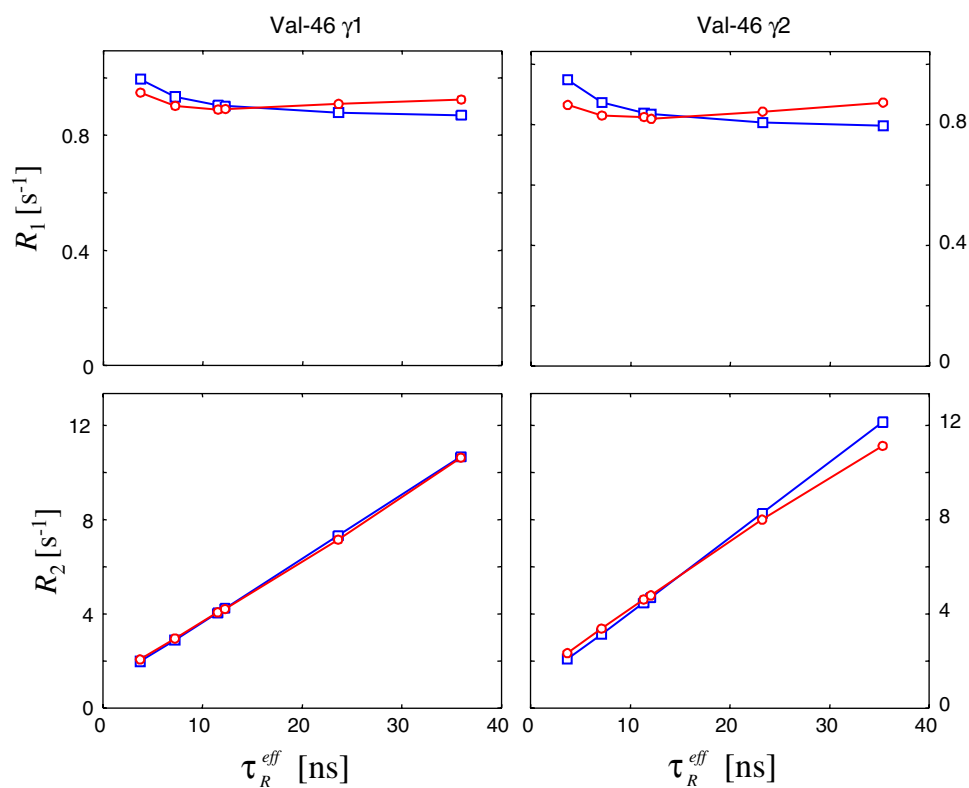

Fig. 6 Fitting of the methyl ^{13}C relaxation data from Val-46 γ1 and γ2 with LS-2(m) model. In addition to Val-46, class C also includes Val-23, Leu-31 δ1, and, tentatively, Val-53 and Val-58

possibility to study the effect of cosolvents on protein dynamics with high accuracy and exceptional degree of detail.

Finally, the class C methyls are illustrated in Fig. 6. At first glance, the pattern appears to be similar to Fig. 4. The differences, however, become apparent when one compares

Fig. 7 S_f^2 and τ_f parameters as extracted from a point-by-point analysis of the Val-46 relaxation data plotted in Fig. 6
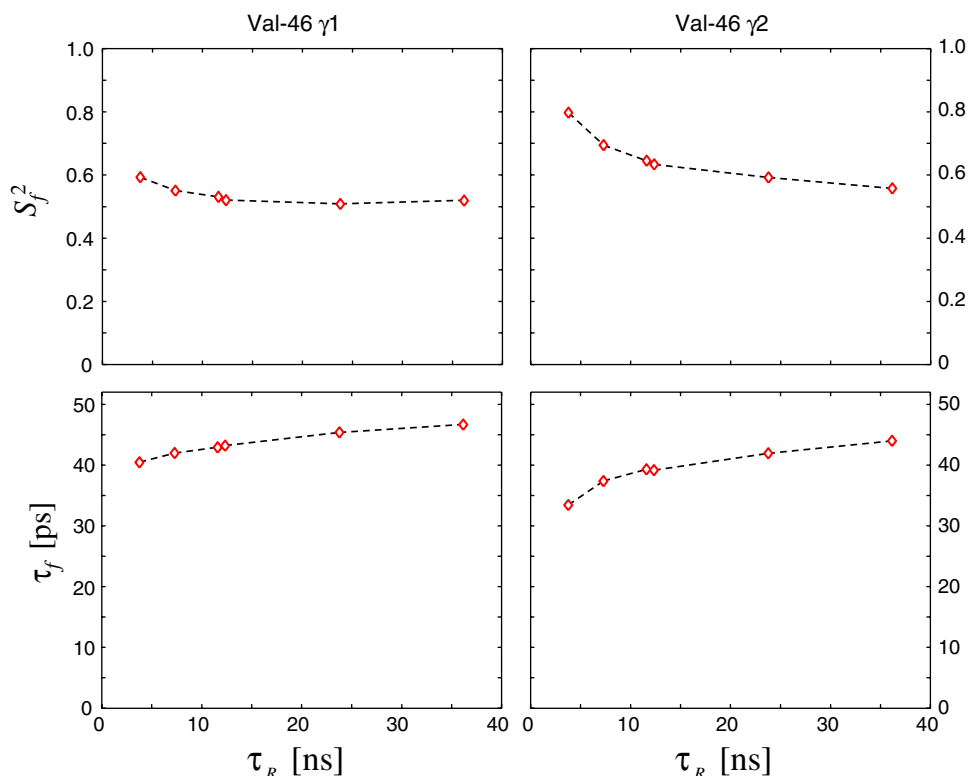
the lower right panels in the two plots. An unexpected trend emerges when the data are analyzed on a point-by-point basis, Fig. 7. Particularly, the plunging S_f^2 profiles appear surprising. Of course, general 'stiffening' of the protein does not necessarily mean that each methyl group becomes constricted. On the contrary, some of them may retain their original mobility (which we believe to be the case for Val-9), while others may even become more mobile (Best et al. 2005; Mittermaier and Kay 2004). However, the combination of the decreasing S_f^2 and increasing τ_f, as seen in Fig. 7, cannot be readily rationalized along these lines. More satisfactory explanation can be arrived at by assuming that the class C methyls are affected by nanosecond time-scale local dynamics. Indeed, a simple simulation where methyl ^{13}C R_1, R_2 data are generated using the LS-4 model and then fitted using the LS-2 model produces the similar descending S_f^2 profiles (not shown). This observation prompted us to turn to the extended data analysis which includes ns time scale motions (see next section).

Methyl ^{13}C relaxation: LS-4 interpretation

A straightforward implementation of the LS-4 model for side-chain methyls assumes that each methyl senses a complex local dynamics parametrized with S_f^2, τ_f, S_s^2, and τ_s. This straightforward version of the extended four-parameter Lipari–Szabo model can be termed LS-4(m). At

the same time it is generally recognized that ns time-scale motions in methyl-bearing side chains mainly occur in a form of rotameric jumps involving torsional angles χ_i (Batchelder et al. 1982; Nicholson et al. 1992; Best et al. 2005). This realization can lead to a more economical description of the motion.

Importantly, in the case of valine, χ_1 rotameric jumps have the same effect on both methyls, $\gamma 1$ and $\gamma 2$. In the case of leucine, the situation is generally more complex. However, a number of scenarios can be described when the two methyls experience the same amount of ns motion: (1) ns rotameric jumps are limited to χ_2 (Best et al. 2005), (2) concerted transitions take place between $(\chi_1, \chi_2) = (300°, 180°)$ and $(180°, 60°)$ (Batchelder et al. 1982; Lovell et al. 2000), (3) ns rotameric jumps are limited to χ_1, whereas χ_2 hops on ps time scale and establishes a conformational equilibrium with roughly equal proportion of $\chi_2 = 180°$ and $60°$ conformers (Hu et al. 2005). All these scenarios are realistic and, taken together, suggest that $\delta 1$ and $\delta 2$ methyls are likely, although not certain, to experience the same effect from ns motion.

The assumption that valine $\gamma 1$ and $\gamma 2$ methyls (and possibly leucine $\delta 1$ and $\delta 2$ methyls) are similarly affected by the ns time scale dynamics can be readily formalized in terms of the Lipari–Szabo model. Specifically, it can be suggested that the relaxation data from both methyls can be fitted simultaneously using the combined set of parameters including $S_f^2(1)$, $\tau_f(1)$, $S_f^2(2)$, $\tau_f(2)$, S_s^2, and τ_s. This model

is designated LS-4(sc-red), where the descriptor indicates that the model applies to the entire *s*ide *c*hain and that the set of parameters is *red*uced by assuming that the S_s^2 and τ_s values are common for the two methyls. For the data set at hand, the LS-4(sc-red) model fits 24 experimental points with 6 fitting parameters.

To test the statistical validity of the obtained results we introduced the counterpart model, LS-2(sc), which operates on the same set of relaxation data as LS-4(sc-red). In essence, the LS-2(sc) model involves consecutive application of the LS-2(m) procedure to the data from the two side-chain methyls, resulting in determination of $S_f^2(1)$, $\tau_f(1)$ and $S_f^2(2)$, $\tau_f(2)$. The residual in the LS-2(sc) model is calculated as a sum of the two individual χ^2 contributions obtained from the LS-2(m) analyses. The Akaike AIC_c measure for both LS-2(sc) and LS-4(sc-red) can be found using (4.1) for which the parameters are listed in Table 1. The statistical Akaike test in this situation is meant to confirm the presence of ns motion, distinguishing it from the conventional Lipari–Szabo dynamics.

The LS-4(sc-red) interpretation was an unqualified success for a single class C side chain, Val-23. The fit of the relaxation data from this residue is shown in Fig. 8. The $\chi^2\left(S_s^2, \tau_s\right)$ map, featuring a well-defined minimum, is displayed in Fig. 9. The AIC difference, $\Delta_i = AIC_c\{$LS-4(sc-red)$\} - AIC_c\{$LS-2(sc)$\}$, was found to be −49.3, which indicates that LS-4(sc-red) is strongly favored over LS-2(sc) [any value under −10 indicates virtual certainty (Burnham
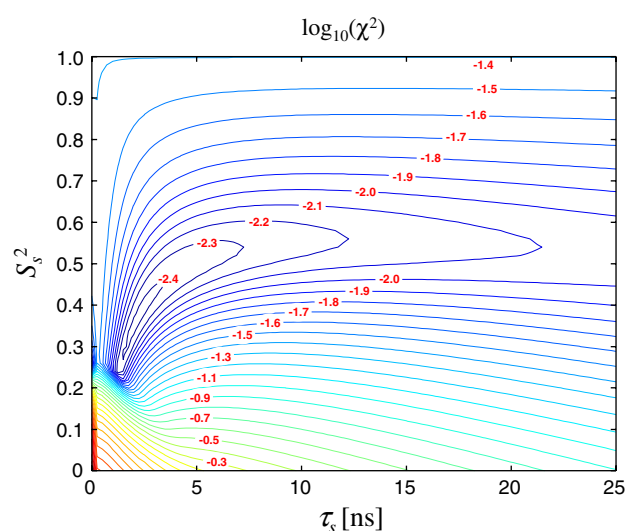

Fig. 9 χ^2 map from fitting of Val-23 $\gamma 1$ and $\gamma 2$ relaxation data with the LS-4(sc-red) model (cf. Fig. 8). The fitting routine was programmed in a form of a grid search in the space of $\left(S_s^2, \tau_s\right)$. At each nod of the grid, the fast-motion parameters, $S_f^2(1)$, $\tau_f(1)$ and $S_f^2(2)$, $\tau_f(2)$, were determined by the standard simplex minimization

and Anderson 2002)]. In summary, this result constitutes a positive detection of nanosecond rotameric jumps in the valine side chain in the experiment using viscogenic cosolvent (glycerol).

The presence of conformational disorder in Val-23 was first noticed by Bernd Reif and co-workers based on the

Fig. 8 Fitting of the methyl ^{13}C relaxation data from Val-23 $\gamma 1$ and $\gamma 2$ with the LS-4(sc-red) model. The fitting residual χ^2 is tenfold lower than in the case of the LS-2(sc) fit (not shown)
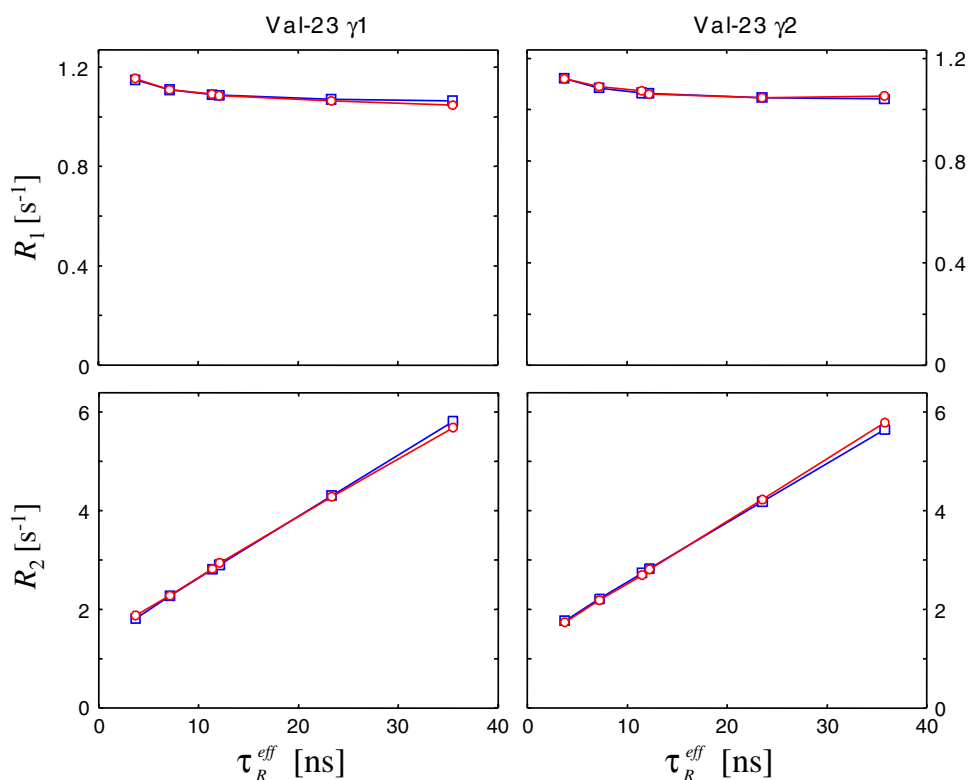
high-resolution crystallographic structure of α-spc SH3 (Chevelkov et al. 2005). Further evidence was obtained from the analysis of the ^{2}H quadrupolar lineshape (Hologne et al. 2005). The amplitude of the slow motion estimated in that study translates into $S_s^2 = 0.72$ (Skrynnikov 2007). Later, a strong evidence of nanosecond dynamics in Val-23 was obtained from the solution-state ^{2}H relaxation study (Reif et al. 2006). The range of dynamic parameters estimated in that work was $S_s^2 = 0.0 - 0.15$ (perhaps, exceedingly low) with $\tau_s = 4.0 - 1.7$ ns at 10°C. This can be compared with $S_s^2 = 0.35$, $\tau_s = 2.0$ ns found in the present study. Considering the fast-motion parameters, the previous estimates were $S_f^2 = 0.69 - 0.87$, $\tau_f = 92 - 80$ ps and $S_f^2 = 0.76 - 0.92$, $\tau_f = 82 - 69$ ps for $\gamma 1$ and $\gamma 2$ methyls, respectively. The current results, obtained at higher temperature, are $S_f^2 = 0.68$, $\tau_f = 45$ ps and $S_f^2 = 0.65$, $\tau_f = 44$ ps. Note that the present work achieves better localization of the χ^2 minimum.

Beyond Val-23, the use of the LS-4(sc-red) model also led to a decrease in fitting residual χ^2 for Leu-31, Val-46, Val-53, and Val-58, i.e. for all class C side chains. For all these residues, however, the improvement was modest, as indicated by the AIC difference Δ_i in the range from +1.3 to +5.2. The AIC scores in this range suggest that the LS-4(sc-red) model is a possible fit for these residues, but less likely than LS-2(sc). The minima in the $\chi^2(S_s^2, \tau_s)$ surfaces are poorly localized and, although the optimized values of S_s^2 and τ_s mostly appear reasonable, it is difficult to attach any significance to these findings.

Considering that in leucine side chains two methyls may not be equivalent with respect to χ_1 rotameric jumps and having Leu-31 in mind, we have also re-analyzed the data using the LS-4(sc) model. In this model the slow-motion parameters are adjusted for the two methyl groups individually, see Table 1. However, the Akaike scores for all residues under consideration turned out to be even poorer (reflecting the increased number of fitting parameters and only marginal improvement in the quality of the fit).

Yet, there is independent evidence suggesting that at least residues Leu-31 and Val-46 are dynamic on the nanosecond time scale. Both of these residues, together with Val-23, adopt multiple conformations in the crystallographic structure 1U06 (Fig. 10). In the solid-state spectrum of α-spc SH3 at 20°C the resonances from Val-46 are missing and the resonances from Leu-31 are extremely weak (Agarwal and Reif 2008). Increasing the temperature to 33°C, while generally causing significant degradation in the quality of the spectrum, improves the conditions for observation of Val-46 and Leu-31 (the former becomes observable, the latter greatly gains in intensity). This outcome can be understood if one assumes that both residues are affected by ns time scale dynamics with long τ_s. In solids, such motion can produce highly unfavorable relaxation rates. Raising
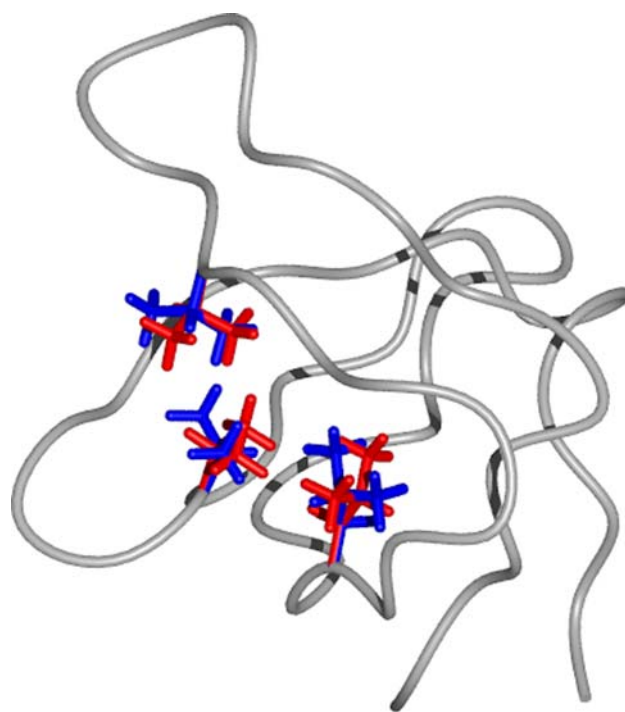

Fig. 10 Alternate conformations of Val-23, Val-46, and Leu-31 side chains in the crystallographic structure 1U06 (Chevelkov et al. 2005). The methyl carbons in the proximal side chains are found within 4 Å from each other

temperature causes a speed-up in dynamics and thus improves the relaxation properties of the methyl spins.

Given that the present study offers tentative evidence of ns time-scale dynamics in Val-46 and Leu-31 and that some indirect confirmation of this result can be obtained from the other sources, it seems quite reasonable to suggest that the motion indeed takes place. If so, why does the proposed method fail to identify this motion in a definitive manner? We have already observed that S_f^2 and τ_f have a tendency to increase with the increasing proportion of the glycerol in solution. The same must be generally true for S_s^2 and τ_s. This undesirable effect does not prevent the detection of ns dynamics in the case when it is pronounced (Val-23). However, it becomes an obstacle in the case when the effect is more subtle, i.e. the population of secondary rotameric species is low and the characteristic time of the rotameric jumps is long (Val-46, Leu-31).

Preferential hydration of α-spc SH3 in glycerol-containing solvent

Since the work by Gekko and Timasheff it has been known that proteins are preferentially hydrated in aqueous glycerol solutions (Gekko and Timasheff 1981a, b). More recently, this finding has been confirmed using a number of different spectroscopic techniques (Courtenay et al. 2000; Roche et al. 2006; Sinibaldi et al. 2007). The partial

expulsion of glycerol from the solvation shell happens as a result of a complex interplay of various factors that have to do with both enthalpy and entropy. These factors also explain the increase in protein stability observed in aqueous glycerol solutions: while the entry of glycerol molecules into the solvation shell of a folded protein is thermodynamically unfavorable, it is even more unfavorable in the case of the unfolded protein with its bigger solvent accessible surface area.

In an apparent paradox, our data presented in Fig. 2 do not show any evidence of preferential hydration. Indeed, it appears that the protein tumbling time is determined by the viscosity of the *bulk solvent* rather than the viscosity of the water-enriched solvation shell. Assuming for a moment that the glycerol is sequestered away from the protein surface, one could expect that the protein is initially surrounded by a 'water bubble' and its correlation time τ_R does not change in response to addition of glycerol (horizontal dashed line in the right part of Fig. 2). Indeed, Betting et al. (2001), suggested on the basis of the dielectric relaxation data that the

tumbling time of RNase A in 74% (w/w) glycerol solution is almost the same as in pure water. This assertion, however, is not borne out by the experimental NMR data.

To resolve this apparent paradox we need to briefly discuss the concept of the solvation shell. It is known that the properties of solvation water are different from the properties of the bulk water. In particular, it has been observed both experimentally and in MD simulations that the diffusion of water on a protein surface is significantly slowed down compared to the bulk (Modig et al. 2004; Pal et al. 2002; Dastidar and Mukhopadhyay 2003; Bizzarri and Cannistraro 2002). In the calculation of the hydrodynamic properties of proteins it has been found necessary to include the hydration layer with effective thickness of 1–3 Å and treat it as an integral part of the protein (Venable and Pastor 1988; Allison and Tran 1995; de la Torre et al. 2000a). The same logic applies to the water/glycerol solvation shell. The shell is essentially comprised of a single layer of water and glycerol molecules making contact with the protein surface (Baynes and Trout 2003; Sinibaldi et al.
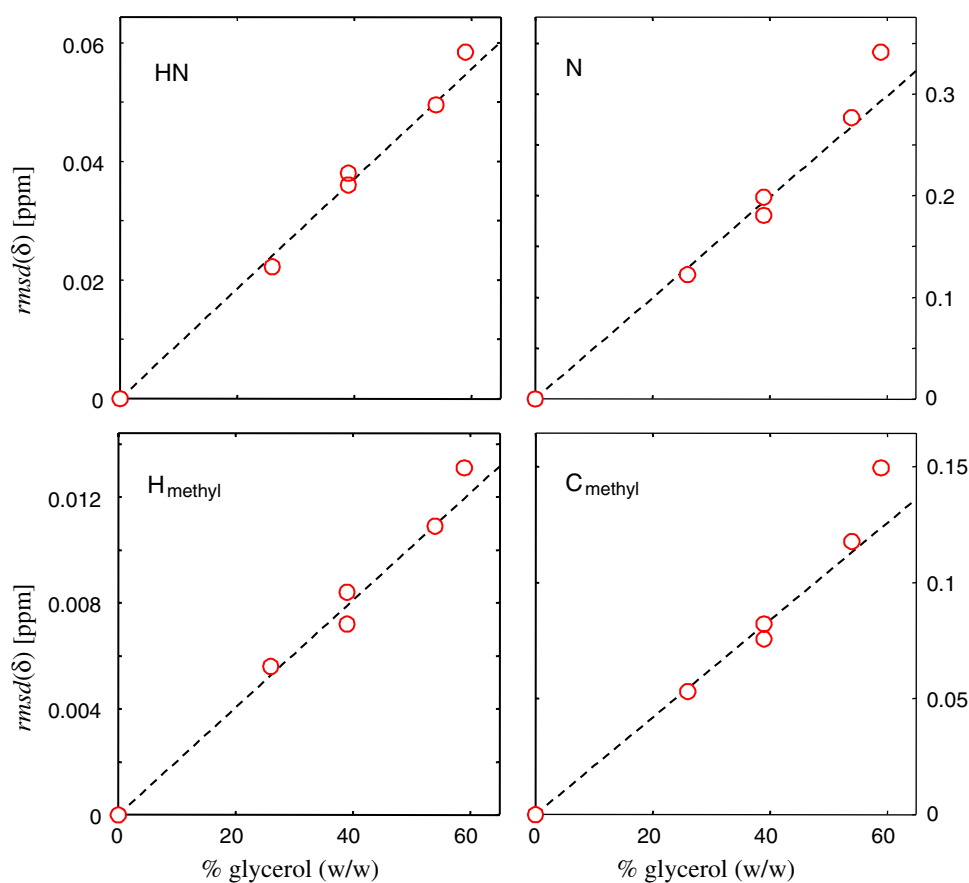

Fig. 11 Chemical shift titration of α-spc SH3 with glycerol. Prior to calculating the chemical shift *rmsd*, we subtract out the spectral 'center of mass': $\delta_i^*(x) = \delta_i(x) - \bar{\delta}(x)$, where $\delta_i(x)$ is the chemical shift of *i*-th resonance in the sample with the fraction of glycerol *x*. The variation of the chemical shift is then quantitated through $rmsd(\delta) = \left[(1/n) \sum_{i=1}^{n} \left(\delta_i^*(x) - \delta_i^*(0) \right)^2 \right]^{1/2}$. This method for comparison of chemical shifts is used to avoid potential complications involving lock frequency in the solvent with variable concentration of deuterated glycerol

2007)—it is far from a spacious 'water bubble' envisaged by some investigators. From the perspective of τ_R determination, the shell should be treated as an integral part of the protein. *It is the viscosity of the bulk solvent on the outside of the thin solvation shell that controls protein tumbling.* The exact composition of the solvation shell, which contains a higher proportion of water and a lower proportion of glycerol than the bulk solvent, does not seem to be important in this context. With this sort of rationale, we conclude that the result in Fig. 2 does not contradict the preferential hydration hypothesis.

The data in Fig. 2 can be used to characterize the nature of the solvation process further. The dependence of τ_R on solvent viscosity appears to be linear up to ca. 55–60% of glycerol, where a departure from linearity is noted. A single point that falls off the straight line in Fig. 2 could be easily discounted as a sample preparation artefact. However, the same trend is observed when chemical shifts are analyzed as a function of glycerol content, Fig. 11. In a standard titration experiment, chemical shifts change linearly as a function of ligand concentration provided that: (1) ligand binding is a simple two-state process and (2) it occurs in the fast-exchange regime. In the case of the water/glycerol solution the interaction of the protein with glycerol is nonspecific and certainly meets the definition of fast exchange (Gekko and Timasheff 1981b; Charron et al. 2002). The linear dependence in the graphs Fig. 11 is, therefore, not surprising. The deviation from linearity, on the other hand, could be potentially significant. It does not seem likely that this deviation is caused by higher-than-intended glycerol concentration of the sample. Rather it may hint at a certain structural transition that begins to be sensed above 55% glycerol concentration (e.g. 'vitrification' of solvent due to the formation of glycerol–glycerol hydrogen bonding network). Of note, the deviation is observed when NMR parameters (chemical shifts, τ_R) are correlated with non-NMR variables (fraction of glycerol, viscosity). In the case when NMR parameters are correlated among themselves the relationship remains linear (cf. Fig. 5). This can be expected as different NMR parameters should change in concert in response to the presumed change in solvation.

Conclusion

Many organisms, such as certain species of yeast, algae, and amphibians, produce glycerol to protect the cells against the environmental stress (Ben-Amotz and Avron 1973; Albertyn et al. 1994; Feder and Burggren 1992). In some cases, the intracellular concentration of glycerol reaches 2.1 M (ca. 23% w/w). At this concentration glycerol should have substantial influence on stability and function of many cytosolic

proteins. These aspects are also of interest in the context of clinical practices where tissues and organs are perfused with glycerol solution prior to being frozen (cryopreservation; Pegg 2007). Another strong reason to be interested in protein–glycerol interactions is the wide use of glycerol in the laboratory setting in biochemistry and structural biology. For example, a recent survey showed that glycerol was used in 50% of all reported cryoprotected crystals (Garman and Doublie 2003). Often the structure stabilizing effect of glycerol has been found beneficial and even essential for successful protein crystallization (Sousa 1995). The influence of glycerol on the crystallographic structure has been a subject of a special study (Charron et al. 2002).

In this work we exploit the viscogenic properties of glycerol to slow down the protein overall tumbling and thus expand the window for observation of nanosecond time-scale internal dynamics. Ideally, the use of the water/glycerol solvent allows to treat the tumbling correlation time τ_R as an isolated experimentally controlled variable (akin to the magnetic field strength, but with a wider dynamic range). In our study the relaxation data have been collected from both backbone ^{15}N and side-chain methyl ^{13}C spins—the former were used to determine τ_R and the latter to probe internal motions. As anticipated, this approach allows for positive identification of ns time-scale rotameric jumps in those side chains where this form of motion is well pronounced. In other cases, where the effect is more subtle, only tentative identification is possible. The main obstacle facing this method is the slight but noticeable 'stiffening' of the protein that occurs upon addition of glycerol. In our study we have been able to demonstrate this stiffening effect as sensed by the individual methyl groups.

Our data suggest that τ_R is dictated by the viscosity of the bulk solvent, rather than the microviscosity of the solvation shell (which has a higher content of water). This can be understood by noticing that the solvation layer is thin and, from the perspective of τ_R determination, should be treated as a part of the protein. It appears that the character of solvation does not change up to 55% (w/w) glycerol concentration. This augurs well for crystallographic studies that typically use 25–30%, and occasionally up to 45%, concentration of glycerol (Garman and Doublie 2003). Given that glycerol causes only modest changes in local dynamics, we also feel optimistic about the possibility of the comparative studies of protein motions by means of the solution- and solid-state NMR (Agarwal et al. 2008) in the samples containing glycerol.

References

Agarwal V, Reif B (2008) Residual methyl protonation in perdeu-terated proteins for multi-dimensional correlation experiments in MAS solid-state NMR spectroscopy. J Magn Reson 194:16–24

Agarwal V, Xue Y, Reif B, Skrynnikov NR (2008) Protein side-chain dynamics as observed by solution- and solid-state NMR spectroscopy: a similarity revealed. J Am Chem Soc 130:16611–16621

Akaike H (1973) Information theory and an extension of the maximum likelihood principle. In: Petrov BN, Csaki F (eds) Second international symposium on information theory. Akademiai Kiado, Budapest, 267–281

Albertyn J, Hohmann S, Thevelein JM, Prior BA (1994) Gpd1, which encodes gycerol-3-phosphate dehydrogenase, is essential for growth under osmotic stress in Saccharomyces cerevisiae, and its expression is regulated by the high-osmolarity glycerol response pathway. Mol Cell Biol 14:4135–4144

Allison SA, Tran VT (1995) Modeling the electrophoresis of rigid polyions - application to lysozyme. Biophys J 68:2261–2270

Batchelder LS, Sullivan CE, Jelinski LW, Torchia DA (1982) Characterization of leucine side-chain reorientation in collagen fibrils by solid-state ^{2}H NMR. Proc Natl Acad Sci USA 79:386–389

Baynes BM, Trout BL (2003) Proteins in mixed solvents: a molecular-level perspective. J Phys Chem B 107:14058–14067

Ben-Amotz A, Avron M (1973) The role of glycerol in osmotic regulation of the halophilic alga Dunaliella Parva. Plant Physiol 51:875–878

Best RB, Clarke J, Karplus M (2005) What contributions to protein side-chain dynamics are probed by NMR experiments? A molecular dynamics simulation analysis. J Mol Biol 349:185–203

Betting H, Häckel M, Hinz HJ, Stockhausen M (2001) Spectroscopic evidence for the preferential hydration of RNase a in glycerol–water mixtures: dielectric relaxation studies. Phys Chem Chem Phys 3:1688–1692

Bizzarri AR, Cannistraro S (2002) Molecular dynamics of water at the protein-solvent interface. J Phys Chem B 106:6617–6633

Blanco FJ, Ortiz AR, Serrano L (1997) ^{1}H and ^{15}N NMR assignment and solution structure of the SH3 domain of spectrin: comparison of unrefined and refined structure sets with the crystal structure. J Biomol NMR 9:347–357

Burnham KP, Anderson DR (2002) Model selection and multimodel interference: a practical information-theoretic approach. Springer, New York

Butler SL, Falke JJ (1996) Effects of protein stabilizing agents on thermal backbone motions: a disulfide trapping study. Biochemistry 35:10595–10600

Caliskan G, Mechtani D, Roh JH, Kisliuk A, Sokolov AP, Azzam S, Cicerone MT, Lin-Gibson S, Peral I (2004) Protein and solvent dynamics: how strongly are they coupled? J Chem Phys 121:1978–1983

Castellani F, van Rossum B, Diehl A, Schubert M, Rehbein K, Oschkinat H (2002) Structure of a protein determined by solid-state magic-angle-spinning NMR spectroscopy. Nature 420:98–102

Charron C, Kadri A, Robert MC, Giege R, Lorber B (2002) Crystallization in the presence of glycerol displaces water molecules in the structure of thaumatin. Acta Crystallogr D Biol Crystallogr 58:2060–2065

Chemical Rubber Company (1948) Handbook of chemistry and physics. Chemical Rubber Publishing, Cleveland

Chen JH, Brooks CL, Wright PE (2004) Model-free analysis of protein dynamics: assessment of accuracy and model selection protocols based on molecular dynamics simulation. J Biomol NMR 29:243–257

Chevelkov V, Faelber K, Diehl A, Heinemann U, Oschkinat H, Reif B (2005) Detection of dynamic water molecules in a microcrystalline sample of the SH3 domain of α-spectrin by MAS solid-state NMR. J Biomol NMR 31:295–310

Chevelkov V, Zhuravleva AV, Xue Y, Reif B, Skrynnikov NR (2007) Combined analysis of ^{15}N relaxation data from solid- and solution-state NMR spectroscopy. J Am Chem Soc 129:12594–12595

Clarkson MW, Lee AL (2004) Long-range dynamic effects of point mutations propagate through side chains in the serine protease inhibitor eglin c. Biochemistry 43:12448–12458

Clore GM, Driscoll PC, Wingfield PT, Gronenborn AM (1990a) Analysis of the backbone dynamics of interleukin 1β using two-dimensional inverse detected heteronuclear 15N–1H NMR spectroscopy. Biochemistry 29:7387–7401

Clore GM, Szabo A, Bax A, Kay LE, Driscoll PC, Gronenborn AM (1990b) Deviations from the simple two-parameter model-free approach to the interpretation of ^{15}N nuclear magnetic relaxation of proteins. J Am Chem Soc 112:4989–4991

Cole R, Loria JP (2003) FAST-modelfree: a program for rapid automated analysis of solution NMR spin-relaxation data. J Biomol NMR 26:203–213

Cornilescu G, Bax A (2000) Measurement of proton, nitrogen, and carbonyl chemical shielding anisotropies in a protein dissolved in a dilute liquid crystalline phase. J Am Chem Soc 122:10143–10154

Courtenay ES, Capp MW, Anderson CF, Record MT (2000) Vapor pressure osmometry studies of osmolyte-protein interactions: Implications for the action of osmoprotectants in vivo and for the interpretation of "osmotic stress" experiments in vitro. Biochemistry 39:4455–4471

Dastidar SG, Mukhopadhyay C (2003) Structure, dynamics, and energetics of water at the surface of a small globular protein: a molecular dynamics simulation. Phys Rev E 68

de la Torre JG, Huertas ML, Carrasco B (2000a) Calculation of hydrodynamic properties of globular proteins from their atomic-level structure. Biophys J 78:719–730

de la Torre JG, Huertas ML, Carrasco B (2000b) HYDRONMR: prediction of NMR relaxation of globular proteins from atomic-level structures and hydrodynamic calculations. J Magn Reson B 147:138–146

Farrow NA, Muhandiram R, Singer AU, Pascal SM, Kay CM, Gish G, Shoelson SE, Pawson T, Forman-Kay JD, Kay LE (1994) Backbone dynamics of a free and a phosphopeptide-complexed src homology two domain studied by ^{15}N NMR relaxation. Biochemistry 33:5984–6003

Feder ME, Burggren WW (eds) (1992) Environmental physiology of the amphibians. University of Chicago Press, Chicago

Fenimore PW, Frauenfelder H, McMahon BH, Parak FG (2002) Slaving: solvent fluctuations dominate protein dynamics and functions. Proc Natl Acad Sci USA 99:16047–16051

Finerty PJ, Muhandiram R, Forman-Kay JD (2002) Side-chain dynamics of the SAP SH2 domain correlate with a binding hot spot and a region with conformational plasticity. J Mol Biol 322:605–620

Foord RL, Leatherbarrow RJ (1998) Effect of osmolytes on the exchange rates of backbone amide protons in proteins. Biochemistry 37:2969–2978

Frederick KK, Marlow MS, Valentine KG, Wand AJ (2007) Conformational entropy in molecular recognition by proteins. Nature 448:325–329

Garman EF, Doublie S (2003) Cryocooling of macromolecular crystals: optimization methods. Methods Enzymol 368:188–216

Gekko K, Timasheff SN (1981a) Mechanism of protein stabilization by glycerol - preferential hydration in glycerol–water mixtures. Biochemistry 20:4667–4676

Gekko K, Timasheff SN (1981b) Thermodynamic and kinetic examination of protein stabilization by glycerol. Biochemistry 20:4677–4686

Goto NK, Gardner KH, Mueller GA, Willis RC, Kay LE (1999) A robust and cost-effective method for the production of Val, Leu, Ile-δ1 methyl-protonated ^{15}N, ^{13}C, ^{2}H-labeled proteins. J Biomol NMR 13:369–374

Hansen DF, Kay LE (2007) Improved magnetization alignment schemes for spin-lock relaxation experiments. J Biomol NMR 37:245–255

Hologne M, Faelber K, Diehl A, Reif B (2005) Characterization of dynamics of perdeuterated proteins by MAS solid-state NMR. J Am Chem Soc 127:11208–11209

Hu H, Clarkson MW, Hermans J, Lee AL (2003) Increased rigidity of eglin c at acidic pH: evidence from NMR spin relaxation and MD simulations. Biochemistry 42:13856–13868

Hu H, Hermans J, Lee AL (2005) Relating side-chain mobility in proteins to rotameric transitions: insights from molecular dynamics simulations and NMR. J Biomol NMR 32:151–162

Hurvich CM, Tsai CL (1989) Regression and time-series model selection in small samples. Biometrika 76:297–307

Igumenova TI, Lee AL, Wand AJ (2005) Backbone and side chain dynamics of mutant calmodulin-peptide complexes. Biochemistry 44:12627–12639

Ishima R, Petkova AP, Louis JM, Torchia DA (2001) Comparison of methyl rotation axis order parameters derived from model-free analyses of ^{2}H and ^{13}C longitudinal and transverse relaxation rates measured in the same protein sample. J Am Chem Soc 123:6164–6171

Johnson E, Chazin WJ, Rance M (2006) Effects of calcium binding on the side-chain methyl dynamics of calbindin D_{9k}: a ^{2}H NMR relaxation study. J Mol Biol 357:1237–1252

Kay LE, Muhandiram DR, Farrow NA, Aubin Y, Forman-Kay JD (1996) Correlation between dynamics and high affinity binding in an SH2 domain interaction. Biochemistry 35:361–368

Kempkes R, Stofko E, Lam K, Snell EH (2008) Glycerol concentrations required for the successful vitrification of cocktail conditions in a high-throughput crystallization screen. Acta Crystallogr D Biol Crystallogr 64:287–301

Knubovets T, Osterhout JJ, Connolly PJ, Klibanov AM (1999) Structure, thermostability, and conformational flexibility of hen egg-white lysozyme dissolved in glycerol. Proc Natl Acad Sci USA 96:1262–1267

Korchuganov DS, Gagnidze IE, Tkach EN, Schulga AA, Kirpichnikov MP, Arseniev AS (2004) Determination of protein rotational correlation time from NMR relaxation data at various solvent viscosities. J Biomol NMR 30:431–442

Korzhnev DM, Skrynnikov NR, Millet O, Torchia DA, Kay LE (2002) An NMR experiment for the accurate measurement of heteronuclear spin-lock relaxation rates. J Am Chem Soc 124:10743–10753

Lee LK, Rance M, Chazin WJ, Palmer AG (1997) Rotational diffusion anisotropy of proteins from simultaneous analysis of N-15 and C-13(alpha) nuclear spin relaxation. J Biomol NMR 9:287–298

Li YC, Montelione GT (1995) Human type-alpha transforming growth-factor undergoes slow conformational exchange between multiple backbone conformations as characterized by ^{15}N relaxation measurements. Biochemistry 34:2408–2423

Lienin SF, Brüschweiler R, Ernst RR (1998) Rotational motion of a solute molecule in a highly viscous liquid studied by 13C NMR: 1, 3-dibromoadamantane in polymeric chlorotrifluoroethene. J Magn Reson 131:184–190

Lipari G, Szabo A (1982a) Model-free approach to the interpretation of nuclear magnetic resonance relaxation in macromolecules. 1. Theory and range of validity. J Am Chem Soc 104:4546–4559

Lipari G, Szabo A (1982b) Model-free approach to the interpretation of nuclear magnetic resonance relaxation in macromolecules. 2. Analysis of experimental results. J Am Chem Soc 104:4559–4570

Lovell SC, Word JM, Richardson JS, Richardson DC (2000) The penultimate rotamer library. Proteins Struct Funct Genet 40:389–408

Mandel AM, Akke M, Palmer AG (1995) Backbone dynamics of Escherichia coli ribonuclease HI: correlations with structure and function in an active enzyme. J Mol Biol 246:144–163

Millet O, Muhandiram DR, Skrynnikov NR, Kay LE (2002) Deuterium spin probes of side-chain dynamics in proteins. 1. Measurement of five relaxation rates per deuteron in ^{13}C-labeled and fractionally ^{2}H-enriched proteins in solution. J Am Chem Soc 124:6439–6448

Millet O, Mittermaier A, Baker D, Kay LE (2003) The effects of mutations on motions of side-chains in protein L studied by ^{2}H NMR dynamics and scalar couplings. J Mol Biol 329:551–563

Mittermaier A, Kay LE (2004) The response of internal dynamics to hydrophobic core mutations in the SH3 domain from the fyn tyrosine kinase. Protein Sci 13:1088–1099

Modig K, Liepinsh E, Otting G, Halle B (2004) Dynamics of protein and peptide hydration. J Am Chem Soc 126:102–114

Musacchio A, Noble M, Pauptit R, Wierenga R, Saraste M (1992) Crystal structure of a src-homology 3 (SH3) domain. Nature 359:851–855

Nicholson LK, Kay LE, Baldisseri DM, Arango J, Young PE, Bax A, Torchia DA (1992) Dynamics of methyl groups in proteins as studied by proton-detected ^{13}C NMR spectroscopy: application to the leucine residues of staphylococcal nuclease. Biochemistry 31:5253–5263

Pal SK, Peon J, Zewail AH (2002) Biological water at the protein surface: dynamical solvation probed directly with femtosecond resolution. Proc Natl Acad Sci USA 99:1763–1768

Pegg DE (2007) Principles of cryopreservation. Methods Mol Biol 368:39–57

Priev A, Almagor A, Yedgar S, Gavish B (1996) Glycerol decreases the volume and compressibility of protein interior. Biochemistry 35:2061–2066

Rariy RV, Klibanov AM (1997) Correct protein folding in glycerol. Proc Natl Acad Sci USA 94:13520–13523

Reif B, Xue Y, Agarwal V, Pavlova MS, Hologne M, Diehl A, Ryabov YE, Skrynnikov NR (2006) Protein side-chain dynamics observed by solution- and solid-state NMR: comparative analysis of methyl ^{2}H relaxation data. J Am Chem Soc 128:12354–12355

Roche CJ, Guo F, Friedman JM (2006) Molecular level probing of preferential hydration and its modulation by osmolytes through the use of pyranine complexed to hemoglobin. J Biol Chem 281:38757–38768

Sinibaldi R, Ortore MG, Spinozzi F, Carsughi F, Frielinghaus H, Cinelli S, Onori G, Mariani P (2007) Preferential hydration of lysozyme in water/glycerol mixtures: a small-angle neutron scattering study. J Chem Phys 126

Skrynnikov NR (2007) Asymmetric doublets in MAS NMR: coherent and incoherent mechanisms. Magn Reson Chem 45:S161–S173

Skrynnikov NR, Millet O, Kay LE (2002) Deuterium spin probes of side-chain dynamics in proteins. 2. Spectral density mapping and identification of nanosecond time-scale side-chain motions. J Am Chem Soc 124:6449–6460

Sousa R (1995) Use of glycerol, polyols and other protein structure stabilizing agents in protein crystallization. Acta Crystallogr D Biol Crystallogr 51:271–277

Tarek M, Tobias DJ (2008) The role of protein-solvent hydrogen bond dynamics in the structural relaxation of a protein in glycerol versus water. Eur Biophys J Biophys Lett 37:701–709

Tjandra N, Feller SE, Pastor RW, Bax A (1995) Rotational diffusion anisotropy of human ubiquitin from N-15 NMR relaxation. J Am Chem Soc 117:12562–12566

Tjandra N, Wingfield P, Stahl S, Bax A (1996) Anisotropic rotational diffusion of perdeuterated HIV protease from N-15 NMR relaxation measurements at two magnetic fields. J Biomol NMR 8:273–284

Tollinger M, Skrynnikov NR, Mulder FAA, Forman-Kay JD, Kay LE (2001) Slow dynamics in folded and unfolded states of an SH3 domain. J Am Chem Soc 123:11341–11352

Tugarinov V, Kay LE (2005) Quantitative ^{13}C and ^{2}H NMR relaxation studies of the 723-residue enzyme malate synthase G reveal a dynamic binding interface. Biochemistry 44:15970–15977

Tugarinov V, Kanelis V, Kay LE (2006) Isotope labeling strategies for the study of high-molecular-weight proteins by solution NMR spectroscopy. Nat Protoc 1:749–754

Venable RM, Pastor RW (1988) Frictional models for stochastic simulations of proteins. Biopolymers 27:1001–1014

Woessner DE (1962) Nuclear spin relaxation in ellipsoids undergoing rotational brownian motion. J Chem Phys 37:647–654

Xue Y, Pavlova MS, Ryabov YE, Reif B, Skrynnikov NR (2007) Methyl rotation barriers in proteins from ^{2}H relaxation data. Implications for protein structure. J Am Chem Soc 129:6827–6838

Zeeb M, Jacob MH, Schindler T, Balbach J (2003) ^{15}N relaxation study of the cold shock protein CspB at various solvent viscosities. J Biomol NMR 27:221–234